communications materials

A Nature Portfolio journal

Article

https://doi.org/10.1038/s43246-026-01089-x

Sustainable rare earth extraction from phytomining by rapid electrothermal calcination

Mingyue Xu[1], Bing Deng[1,2] ✉, Erkang Feng[1], Teng Wang[1,3], Zefang Yin[1], Ziyu Huang[1], Wen-Shen Liu[4], Xianlai Zeng[1,2], Lena Q. Ma[5], Rongliang Qiu[4] & Jianguo Liu[1,2] ✉

Rare earth elements (REE) are indispensable to the clean energy and advanced electronics industries, yet conventional mining often entails substantial environmental and energy costs. Phytomining, which harnesses the ability of hyperaccumulator plants to concentrate REE from soil, offers a promising sustainable alternative. However, the downstream recovery of REE from plant biomass remains inefficient and resource-intensive. In this study, we introduce a rapid electrothermal calcination (REC) strategy for REE-enriched biomass, which enables fast thermal activation (e.g., 1000 °C for 20 s) and improves REE extractability through dilute acid leaching, with extraction efficiencies of up to ~97%. The REC process is versatile across various organic hyperaccumulator matrices, as demonstrated using *Blechnum orientale* and *Dicranopteris linearis*. Comparative life-cycle analyses reveal that REC reduces carbon emissions by over 70% relative to conventional furnace-based methods. These results establish REC as a sustainable and scalable platform for advancing circular REE recovery via phytomining.

Critical minerals underpin the technological infrastructure essential to achieving UN Sustainable Development Goals[1]. Among these mineral resources, rare earth elements (REE) constitute critical raw materials for modern high-tech industries, with widespread applications in renewable energy systems, electric vehicles, and advanced electronics[2]. In the global technological landscape, current industrial extraction routes are dominated by bastnäsite and ion-adsorption clays. While these approaches enable large-scale supply, they are constrained by high energy demand, heavy reliance on chemical reagents[3], environmental burdens, and substantial costs associated with wastewater and acid treatment (Supplementary Table 1)[4]. Beyond energy consumption and greenhouse gas emissions, traditional mining processes also face the challenge of substantial water pollution, generating approximately 40.48 kL of wastewater per kilogram of REE produced[5]. As a result, achieving efficient and environmentally sustainable extraction of REE has become an urgent technological challenge worldwide. In recent years, both academia and industry have actively explored alternative technologies, including bioleaching[6], green chemical processes[7], and rapid electrothermal treatments[8], to reduce environmental impacts and improve economic viability.

China has dominated global REE production[4], contributing over 90% of the world supply[9], primarily from ion-adsorption deposits (IADs) in weathered granitic terrains[8,10]. With the diminishing availability of high-grade IADs, there is an urgent need to recover REE from other resources[11]. Vegetation naturally colonizing these IADs has revealed a promising solution: certain plant species exhibit exceptional REE hyperaccumulation capabilities[12]. For instance, some ferns achieve shoot REE concentrations exceeding 3000 mg kg^{-1} (dry weight), a 45-fold enrichment compared to surrounding soils[13]. Hyperaccumulator species, characterized by their capacity to concentrate metals above 0.1 wt% in aerial tissues, are capable of thriving on marginal lands while sustaining scalable biomass yields[14]. This unique ecological adaptation makes them particularly well suited for phytomining[15], an emerging strategy that integrates metal recovery with ecosystem restoration[16].

[1]School of Environment, Tsinghua University, Beijing, China. [2]State Key Laboratory of Iron and Steel Industry Environmental Protection, Tsinghua University, Beijing, China. [3]Tanwei College, Tsinghua University, Beijing, China. [4]School of Environmental Science and Engineering, Guangdong Provincial Key Laboratory of Environmental Pollution Control and Remediation Technology, and Guangdong Provincial Engineering Research Center for Heavy Metal Contaminated Soil Remediation, Sun Yat-sen University, Guangzhou, China. [5]Institute of Soil and Water Resources and Environmental Science, College of Environmental and Resource Sciences, and State Key Laboratory of Soil Pollution Control and Safety, Zhejiang University, Hangzhou, China. ✉e-mail: dengbing@tsinghua.edu.cn; jgliu@tsinghua.edu.cn

Phytomining leverages plant uptake to transfer soil-bound REE into harvestable biomass, followed by target element recovery[17,18]. Current industrial workflows, however, remain constrained by inefficient post-harvest processing[19,20]. For example, conventional ash-based methods involve furnace incineration at 550 °C for 3 h, which achieves only 65–85% REE liberation efficiency[11]. Subsequent leaching with concentrated acids generates 3–5 L of acidic effluent per kg of biomass, requiring costly neutralization[21]. While recent advances in selective elution (e.g., citric acid at pH 2.5) have improved REE purity to ~80%, these methods still suffer from co-dissolution of Fe^{3+} and Al^{3+} (20–30% contamination), necessitating further purification steps[11]. Hence, a rapid and energy-efficient pretreatment is imperative for the REE extraction from hyperaccumulators.

To address the limitations of traditional phytomining workflows, recent efforts have explored alternative pretreatment strategies that can more efficiently liberate REE from plant biomass while minimizing energy and environmental costs. Among them, electrothermal techniques have shown promise due to their rapid heating rates and reduced energy consumption[22]. These methods, originally developed for materials synthesis[23], offer a different thermal environment compared to conventional furnaces[24]. Although flash Joule heating has previously been employed to recover critical metals from industrial residues such as coal fly ash and electronic waste[21], its application to organic biomass, particularly REE-hyperaccumulating plants, has remained largely unexplored[25,26]. Importantly, plant tissues differ from mineral or industrial waste matrices in their morphology, thermal behavior, and REE-hosting mechanisms, suggesting the need for tailored optimization approaches[27].

Herein, we report a rapid electrothermal calcination (REC) method tailored for phytomining biomass, which enables efficient REE liberation from plant tissues under short treatment times (~ 20 s at ~1000 °C). Unlike previous studies that focused on REE recovery from inorganic materials, this work pioneers the application of REC to plant-derived sources, leveraging their unique structural and compositional characteristics. Through systematic comparison with conventional furnace calcination (typically operated for 3 h)[14], we demonstrate that REC enhances REE extractability using only dilute acid, achieving >97% recovery efficiency while substantially reducing energy consumption by >70% as well as cost. Furthermore, REC achieves low Fe/Al impurity levels of ~0.4 wt%. Notably, we show the generalizability of this approach across multiple hyperaccumulator species, including both *Blechnum orientale* and *Dicranopteris linearis*. By combining a plant-based resource with an electrothermal activation pathway, our study provides a potential approach toward developing phytomining technologies that may contribute to sustainable agriculture, clean energy, and circular economy objectives. Importantly, phytomining is positioned as an ecological restoration strategy and a supplementary source of REE, rather than a replacement for conventional mining, thereby enhancing its compatibility with broader sustainability agendas. Taking into account the global supply chain structure, operating expenditure, life-cycle environmental indicators, and policy, as well as land-use constraints, this study demonstrates that REC can serve as a low-carbon and economically competitive supplementary source of REE in regions with abundant hyperaccumulator resources. In particular, techno-economic analysis reveals that phytomining offers lower capital expenditure compared with industrial bastnäsite and ion-adsorption clay routes, and achieves lower overall costs relative to conventional furnace calcination. Potential applications include the recovery of REE from marginal lands or agricultural residues, thereby aligning resource development with environmental sustainability and social equity objectives.

Results

REE extraction from *Blechnum orientale* by electrothermal activation

The process of extracting REE from REE-enriched plants is illustrated in Fig. 1a. *Blechnum orientale* (BO), a representative REE-enriched plant grown in ion-adsorption-type rare earth deposits in China[28], was used as the feedstock material (Fig. 1b). Scanning electron microscopy (SEM) images reveal that the overall structure of BO is tightly encapsulated (Fig. 1c). REE store both within the cells and adsorbed on the cell walls or precipitated in the intercellular spaces[29], exhibiting two distinct compartmentalization effects. X-ray fluorescence (XRF) and elemental analysis results indicate that the major constituents of the raw BO material (Raw BO) are C (39.4%), O (33.7%), Si (6.7%), Ca (6.4%), and H (5.6%) (Supplementary Table 2). Thermogravimetric analysis (TGA) results (Fig. 1d) show that most of the organic matter in Raw BO decomposes below 600°C, with a total mass loss of 89%. The decomposition process was observed in three stages: (i) evaporation of adsorbed water, (ii) combustion of cellulose, and (iii) combustion of hemicellulose and lignin[14], corresponding to the three peaks of the first derivative plot (Fig. 1d).

In a typical electrothermal activation process, naturally air-dried Raw BO was ground into a powder and then loaded on a carbon paper heater (Fig. 1e). High-voltage discharges from the power source heat the carbon heater to elevated temperatures. In a typical discharge process, the corresponding real-time temperature curve shows a rapid heating rate (200 °C s^{-1}) followed by stable heating at ~1000 °C for 20 s (Fig. 1f). During REC, the sample exhibits a relatively uniform temperature distribution, without an apparent gradient (Fig. 1g). The electrical current induces structural reorganization within the plant tissue, thereby loosening tightly bound organic structures into more separable states[30,31], which facilitates subsequent extraction and separation processes[21]. The solid generated following electrothermal activation treatment is designated as Activated BO.

REE leaching from the activated biomass by REC

After the REC reaction, we conducted acid leaching of REE from the residue. First, to establish baseline concentrations, Raw BO was digested with concentrated nitric acid in a microwave digestion system. The concentrations of REE were measured using inductively coupled plasma optical emission spectroscopy (ICP-OES). The total concentrations of REE were quantified to be 3764.4 ppm, with La, Nd, Ce, and Pr concentrations of 1554.5 ppm, 825.8 ppm, 569.0 ppm, and 257.7 ppm, respectively, which account for 85.2% of the total REE content (Fig. 2a and Supplementary Table 3).

Then, we conducted acid leaching of the Activated BO. For comparison, Raw BO, as well as the calcinated BO in a muffle furnace at 550 °C for 3 h (referred to as Calcinated BO), were used. The leachable REE content in all samples was determined via H_2SO_4 leaching. In previous studies, the effect of acid concentration at >1 M on the leaching of REE was found to be limited[21]. Therefore, in this work, we adopted 1 M H_2SO_4 leaching as the standard protocol, as it is more cost-effective. Leaching of Raw BO resulted in a total REE extraction of 82.5% (Supplementary Note 1), with extraction rates of 82.3%, 85.2%, 79.2%, and 85.4% for La, Nd, Ce, and Pr, respectively (Fig. 2b). The Calcinated BO showed a total REE extraction yield of 90.3%, and extraction rates of 89.6%, 89.8%, 95.9%, and 92.2% for La, Nd, Ce, and Pr (Supplementary Table 4). In contrast, a total REE extraction yield of 97.3% was obtained for Activated BO, with the extraction rates for La, Nd, Ce, and Pr in Activated BO reaching 97.8%, 97.9%, 99.3%, and 96.0%, respectively (Fig. 2b and Supplementary Table 5). Hence, the REE extraction yield can be improved by 14.8% with the REC activation.

The pH-dependent leaching dynamics of REE from Raw BO, Activated BO, and Calcinated BO were also investigated (Fig. 2c). In general, the extraction yield decreases as the pH increases (Supplementary Figs. 1–4 and Supplementary Table 6). At pH 0.7, the REE extraction from Activated BO reached 86.6%, which is higher than that of Calcinated BO (77.3%) and Raw BO (~54.3%), and even higher than the extraction rate of Raw BO at higher acid concentrations (e.g., 82.5% at pH 0.3). The rapid REC process contributes to a higher REE extraction yield than the lengthy calcination process. We presume that extended thermal treatment during the calcination process could lead to the evaporative loss of REE with the ash residue[32].

Deviations between different REE were observed, which may be attributed to the uneven distribution of REE in Raw BO and varying degrees of activation among the REE. REC experiments were conducted at temperatures of 500 °C, 600 °C, 700 °C, 800 °C, 900 °C, and 1000 °C, with REE extraction rates exceeding 90% at 900 °C and 1000 °C (Fig. 2d). Further optimization of the reaction time revealed that the extraction rate increased

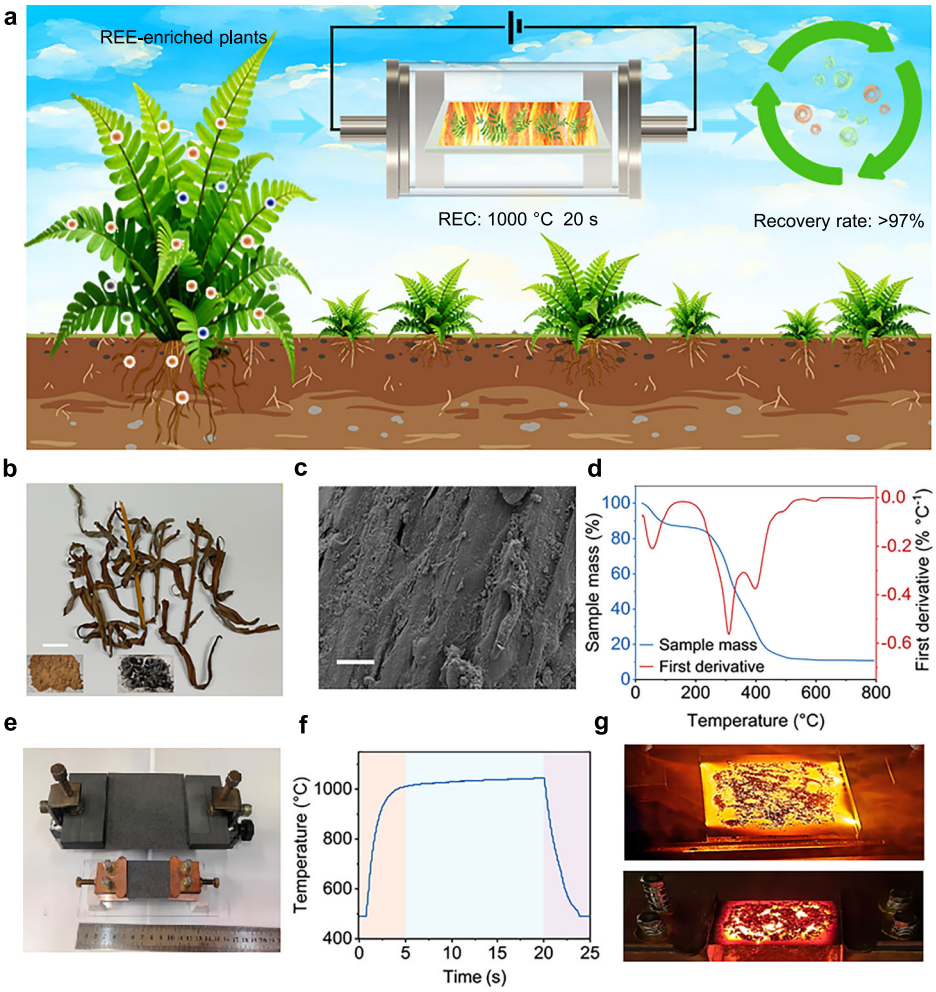

Fig. 1 | Extraction of REE by rapid electrothermal activation. **a** Conceptual schematic of REE extraction from phytomining by REC. **b** Picture of dried *Blechnum orientale* (BO). Scale bar, 3 cm. Inset, the mixture of crushed BO before and after REC. **c** SEM image of dried raw BO materials. Scale bar, 10 μm. **d** Thermogravimetric analysis of BO and the first derivative. **e** Picture of the reactor and an enlarged reactor during the REC process. **f** Real-time temperature curve measured during the REC reaction. **g** Pictures of intense light emission during the REC process.

initially and then decreased with prolonged reaction time. The highest extraction rate, 97.3%, was achieved at 1000 °C with a reaction time of 20 s. However, when the reaction time was extended to 60 s (Fig. 2e), the extraction rate slightly decreased, presumably due to the volatilization of ash[33].

Mechanism of the enhanced leaching of REE by REC

We then studied the mechanism underlying the enhanced REE extraction by REC. First, we used X-ray diffraction (XRD) to reveal the crystallinity and chemical forms[21]. The XRD patterns show substantial differences in the diffraction peaks of Raw BO, Activated BO, and Calcinated BO (Fig. 3a and Supplementary Fig. 5). The diffraction peaks of Raw BO are broad, indicating an amorphous structure. In contrast, the diffraction peaks of Calcinated BO and Activated BO are sharper and more intense, suggesting that furnace calcination improved the crystallinity, due to the recrystallization process of minerals at high temperatures[34]. The crystallinity of the Activated BO was determined to be 12.2%, which was lower than the 15.0% crystallinity of the Calcined BO. Furthermore, Activated BO demonstrated larger carbon crystalline sizes (1.5 nm) compared to those of Calcinated BO (0.7 nm). Conversely, Calcinated BO showed enlarged $CaCO_3$ crystalline size (29.1 nm) relative to Activated BO (21.9 nm). The SEM images of Activated BO (Fig. 3b) reveal pivotal changes in the surface microstructure of the sample. The surface of Raw BO was relatively smooth (Fig. 1c), while after REC treatment, the surface of Activated BO became rougher and more porous. The explosive release of volatiles and thermally-induced microcracking collaboratively establish a hierarchical porous architecture (Fig. 3b and Supplementary Fig. 6), contributing to the acid leaching process[35].

Next, elemental analysis of the REE was performed using energy dispersive X-ray spectroscopy (EDS) (Fig. 3c) and X-ray photoelectron spectroscopy (XPS) (Fig. 3d). The EDS and XPS full spectra of Activated BO showed similar peaks to Calcinated BO, including peaks for oxygen, neodymium, carbon, and silicon. Both are distinct from that of the Raw BO, demonstrating the efficient removal of organics[36]. During FC, the biomass was subjected to prolonged heating (3 h), which facilitated the co-evaporation of ash and certain REE in gaseous form (Supplementary Fig. 7). This volatilization was experimentally confirmed by the recovery of 2.6% of total REE from the crucible lids in muffle furnace trials (Supplementary Table 7). Such evaporative losses inevitably reduced the relative REE content in the Calcinated BO, leading to its lower extraction efficiency compared with the Activated BO[37]. In contrast, the FJH process occurred within only ~10 s, minimizing REE volatilization and thereby retaining more REE in the solid product available for subsequent leaching. This mechanism is illustrated in Supplementary Fig. 8, which schematically highlights the different REE retention behaviors between the two calcination pathways. This underscores the advantages of our REC process, which is completed in seconds and avoids the evaporative loss of REE. The EDS maps show a uniform distribution of REE in all samples (Supplementary Figs. 9–11). According to the XPS fine spectra (Fig. 3e), no La signal was detected in Raw BO, indicating an extremely low surface concentration. In contrast, Activated BO exhibited La signatures in XPS spectra (Fig. 3e). The observed La^{3+} peaks at 834.9 eV demonstrate the predominant formation of lanthanum metal oxide following REC treatment[21]. In addition, the Nd main peak in Raw BO was located at 980.50 eV, with a satellite peak at 977.55 eV and an O KLL peak at 974.10 eV (Fig. 3f)[38]. In Activated BO, the Nd^{3+} main peak was located at 981.32 eV, the satellite peak at 978.44 eV,

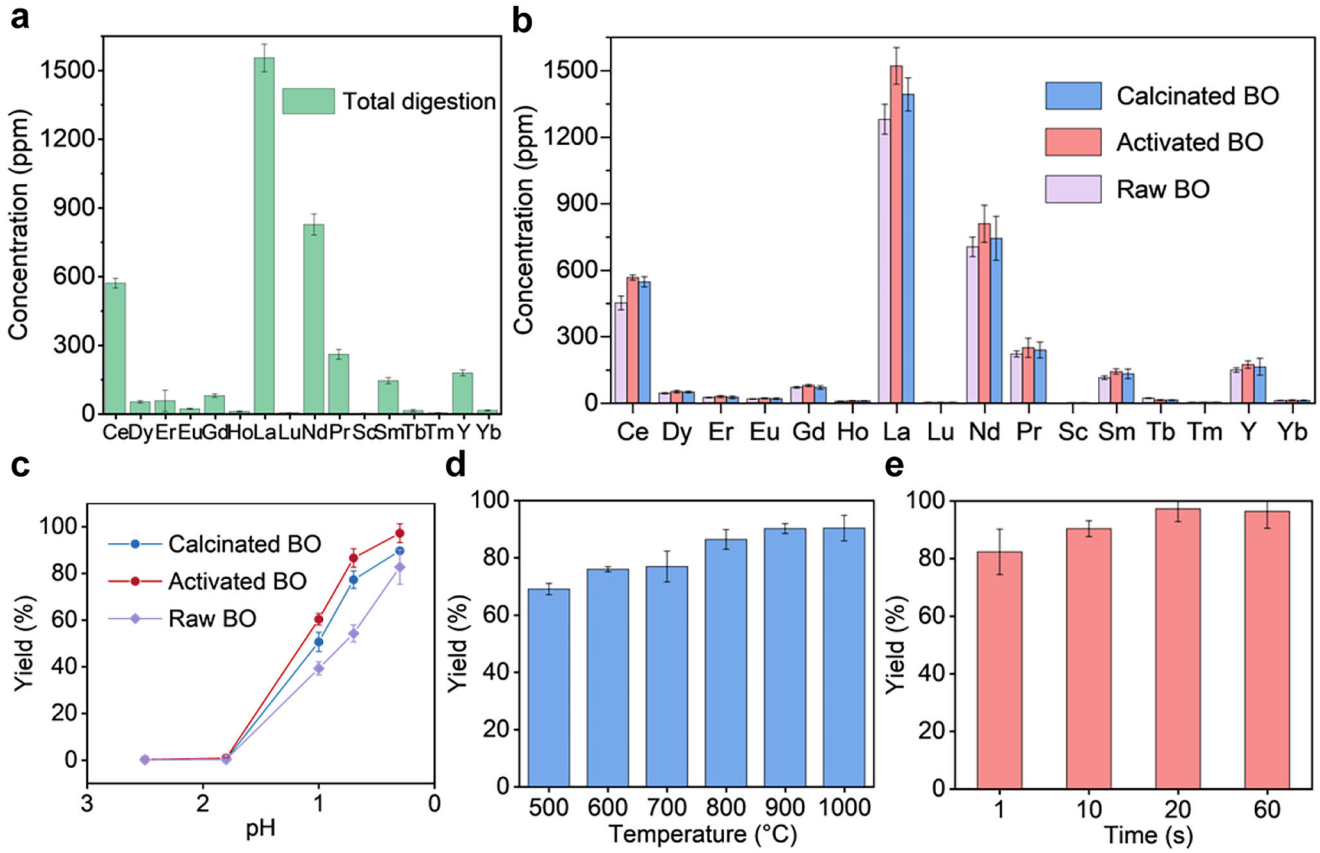

Fig. 2 | Improved extraction yield of REE from BO by electrothermal activation. **a** Total quantification of REE in Raw BO. **b** H_2SO_4-extractable REE contents (1 M, 90 °C) in Raw BO, Activated BO, and Calcinated BO. **c** pH-dependent REE leaching yield from the Raw BO, Activated BO, and Calcinated BO. **d** Extraction yield of REE at different REC reaction temperatures for 10 s. **e** Extraction yield of REE at 1000 °C for different reaction times. All error bars denote standard deviation where $N = 3$.

indicating changes in chemical bonds or electronic structure. The thermal treatment process involves the breaking and reformation of chemical bonds, which in turn affects the chemical state of REE in the samples[39]. The XPS spectra of REE in the Calcinated BO were similar to those of Activated BO (Supplementary Figs. 12, 13).

Lastly, the speciation and phase-partitioning of REE were quantitatively assessed through standardized sequential extraction protocols coupled with ICP-OES analysis (see details in "Materials and Methods", Fig. 3g, h, and Supplementary Figs. 14–17)[40,41]. In the plant, the primary forms of REE were humic acid-bound (60.3%), residue-bound (16.8%), and strongly organic-bound (15.9%). After REC treatment, the proportions shifted to residue-bound (56.0%) and humic acid-bound (41.8%) (Fig. 3g, h), while the strongly organic-bound part was almost eliminated. Similarly, after muffle furnace calcination, the REE distribution was changed to humic acid-bound (66.0%) and residue-bound (33.0%). In natural environments, humic acid-bound REE may exhibit higher bioavailability[34,42]. The REC treatment likely weakened the chemical bonds between organics and REE[43], facilitating the release of strongly organic-bound REE (Fig. 3i). As a result, the REE in the Activated BO could be efficiently extracted under mild acid leaching conditions.

Generality of the REC electrothermal activation process

The electrothermal activation process can be extended to other REE-enriched plants, such as *Dicranopteris linearis* (DL). DL is a pioneering plant in REE mine tailings, known for its strong reproductive capability and fast growth, making it an ideal plant for phytomining[12]. Using DL as the precursor (Supplementary Figs. 18, 19), REC induced a distinct color transition from green to dark gray (Fig. 4a). SEM revealed a densely encapsulated architecture of DL (Fig. 4b). The solid generated following REC treatment is designated as Activated DL. Activated DL exhibited a porous structural morphology (Supplementary Fig. 20). TGA demonstrated that 95.6% of organic constituents in DL underwent near-complete decomposition below 600 °C (Fig. 4c).

The total REE content in DL was determined to be 754 ppm (Fig. 4d), with other major components including C, O, N, Si, Ca, and others (Supplementary Table 8). The extraction of REE from DL was carried out via a direct leaching process using 1 M H_2SO_4 (as detailed in the "Materials and Methods" section). Similar to BO, the extractability of REE from DL after REC electrothermal activation also depends on the REC temperature and duration (Fig. 4e). At the optimized REC temperature and time, the sulfuric acid-extractable REE content increased to ~727 ppm, higher than the ~603 ppm obtained by furnace calcination for 3 h (Fig. 4e). REC experiments were conducted at temperatures of 700 °C, 800 °C, 900 °C, and 1000 °C, with REE extraction rate exceeding 90% at 1000 °C (Fig. 4f). Further optimization of the reaction time revealed that the extraction rate increased initially and then decreased with prolonged reaction time (Fig. 4g). The highest extraction rate, 96.5%, was achieved at 1000 °C with a reaction time of 20 s.

The mechanism for improving REE extraction from DL via the REC process is also studied, which is likely similar to that of BO. The XRD diffractograms of Activated DL and Calcinated DL exhibited analogous crystalline signatures, with prominent diffraction peaks corresponding to calcite-phase $CaCO_3$ (PDF #51-1524) and C (PDF #50-0927), suggesting conserved mineralogical frameworks despite divergent thermal activation mechanisms (Fig. 4h and Supplementary Fig. 21). Elemental characterization using EDS (Supplementary Fig. 22) and XPS (Supplementary Fig. 23) revealed comparable spectral signatures between Activated DL and Calcinated DL, exhibiting characteristic peaks of C, O, and Si. The EDS maps show a uniform distribution of REE in all samples (Supplementary Figs. 24–26). XPS fine spectra (Supplementary Figs. 27, 28) further confirmed analogous chemical interaction patterns in both DL and BO systems.

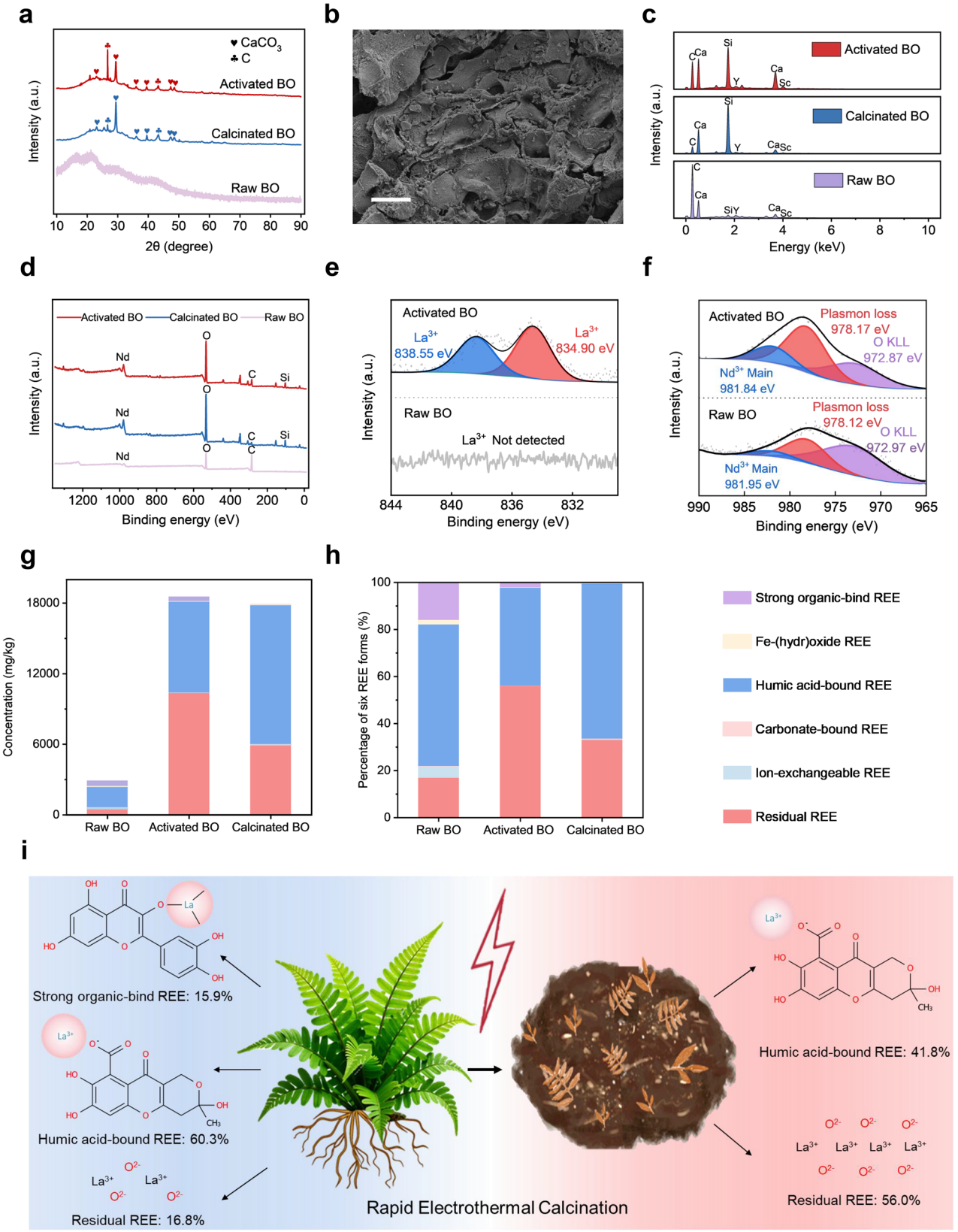

Fig. 3 | Mechanism of the improved REE extractability by the electrothermal activation. **a** XRD patterns of Raw BO, Activated BO, and Calcinated BO. The $CaCO_3$ with reference PDF ($CaCO_3$, #99-0022) and C with reference PDF (C, #26-1080) were shown. **b** SEM image of Activated BO. Scale bar, 10 μm. **c** EDS of Raw BO, Activated BO, and Calcinated BO. **d** XPS full spectra of Raw BO, Activated BO, and Calcinated BO. **e** XPS fine spectra of La $3d_{5/2}$ in Raw BO and Activated BO. La was not detected in Raw BO. Note that the La at 838.55 eV is the shake-up satellite. **f** XPS fine spectrum of Nd $3d_{5/2}$ in Raw BO and Activated BO. The O Auger KLL peak is labeled. **g** Content of six REE forms in Raw BO, Activated BO, and Calcinated BO. **h** Percentage of six REE forms of La in Raw BO, Activated BO, and Calcinated BO. **i** Changes in the percentage of different forms of REE in Raw BO and Activated BO.

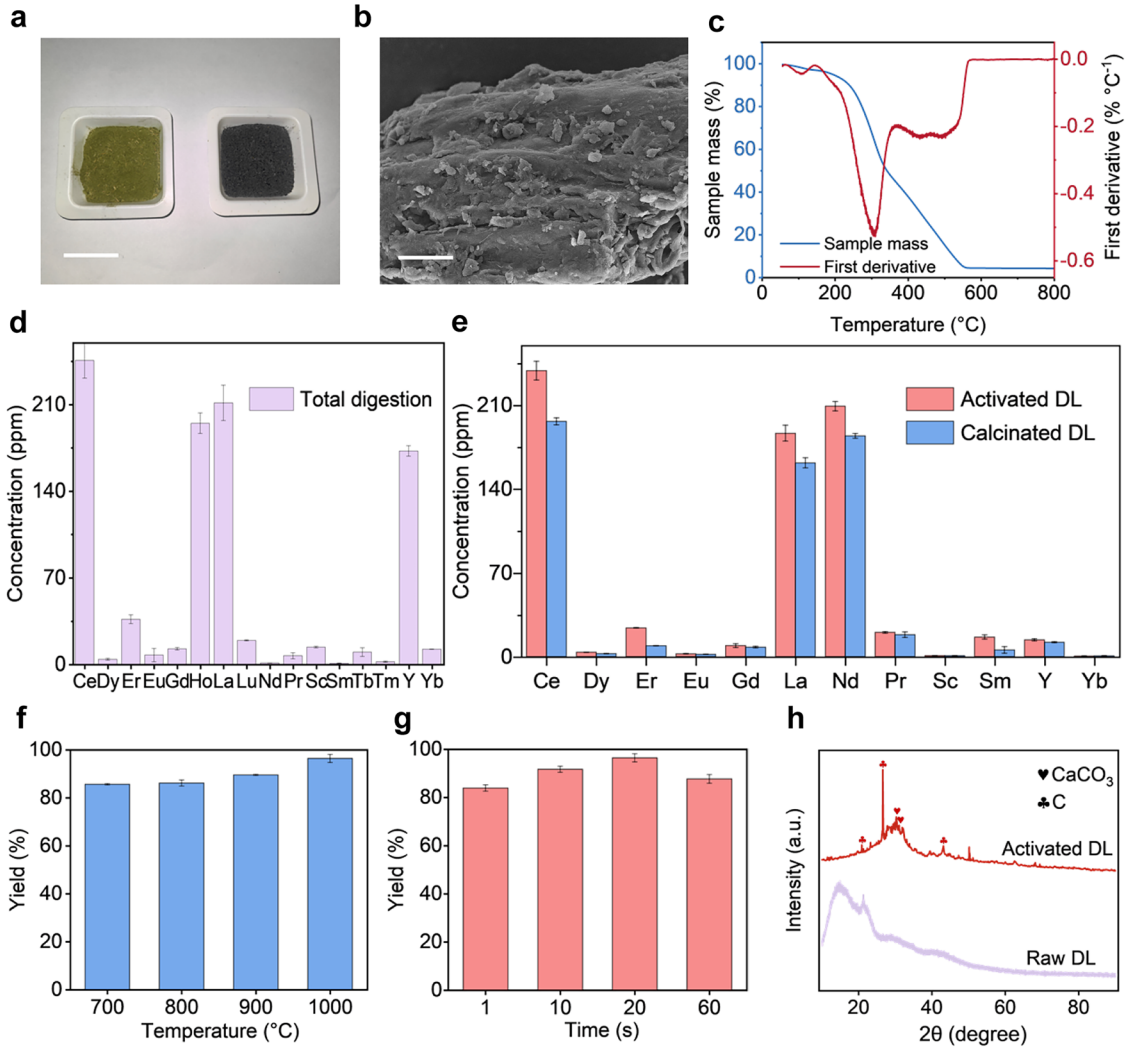

Fig. 4 | Extraction of REE from DL. a Picture of dried *Dicranopteris linearis* (DL). Scale bar, 2 cm. **b** SEM image of dried DL Raw materials. Scale bar, 5 μm. **c** Thermogravimetric analysis of DL and the first derivative. **d** Total quantification of REE in Raw DL. **e** H_2SO_4-extractable REE contents (1 M, 90 °C) of REE in Raw DL, Calcinated DL, and Activated DL. **f** Extraction yield of REE for 10 s at different REC reaction temperatures. **g** Extraction yield of REE at 1000 °C for different reaction times. **h** XRD patterns of Calcinated DL and Activated DL. The $CaCO_3$ with reference PDF ($CaCO_3$, #51-1524) and C with reference PDF (C, #50-0927) were shown. All error bars denote standard deviation where $N = 3$.

The REC process can expose the REE by breaking down the matrix, accelerating the leaching rate and extraction efficiency of the REE.

Life-cycle assessment and technoeconomic analysis

The environmental impacts were evaluated via life cycle assessment (LCA) (Supplementary Note 2 and Supplementary Figs. 29–34). Four scenarios were considered in this study: rapid electrothermal calcination (REC), furnace calcination (FC), Ethylenediaminetetraacetic acid leaching (EDTA), and hydrothermal carbonization (HC) (Fig. 5a). The transporting, drying, and grinding processes for the four scenarios are identical, so they are not taken into consideration in this study. The system boundary includes the input of BO, output of REE leachate, and the process materials and energy consumptions. The functional unit was defined as the production of 1 kg of REE. Life-cycle inventory (LCI) data for inputs were obtained from our lab and the literature (Supplementary Table 8)[44]. The LCI entries were converted into environmental impacts using the ReCiPe 2016 methodology[23]. Monte Carlo simulations were implemented for sensitivity analyses[45] (Supplementary Figs. 35, 36). The energy efficiency of the REC was quantitatively compared with other processes under optimized operational parameters. Due to their higher extraction efficiency, the REC and HC processes require less plant biomass. For processing 1 kg of biomass, REC requires 74.0 kWh of electricity, compared with 288.3 kWh for FC, 143.9 kWh for the EDTA process, and 101.8 kWh for the HC process, highlighting that the electricity demand of REC is only 25.7% of that of FC and demonstrating its improved energy efficiency. Furthermore, four intermediate environmental indicators were analyzed: terrestrial acidification (TA), human toxicity (HT), climate change (CC), and freshwater eutrophication (FE) (Fig. 5b–e, Supplementary Figs. 37, 38, and Supplementary Tables 9–13). The CC impacts for REC, FC, EDTA, and HC were estimated at ~18, ~75, ~43, and ~24 tonnes CO_2-eq., respectively (Fig. 5d and Supplementary Fig. 37). Notably, REC reduced the CC by ~76% compared to FC. Owing to its higher REE extraction efficiency, the REC process requires less sulfuric acid than FC. In addition, its lower electricity consumption leads to reduced impacts in categories such as natural land transformation, land occupation, water depletion, and ecotoxicity, thereby offering advantages over the other three processes (Fig. 5g and Supplementary Figs. 39–43).

The economic feasibility of the REC process was evaluated via technoeconomic analysis (TEA) (Supplementary Note 3). The required chemical reagents were sourced based on domestic market prices in China, with specific prices for relevant items detailed in Supplementary Table 14. The industrial electricity consumption rate was estimated at $0.11 per kWh. In this preliminary analysis, we focused on raw material costs, energy

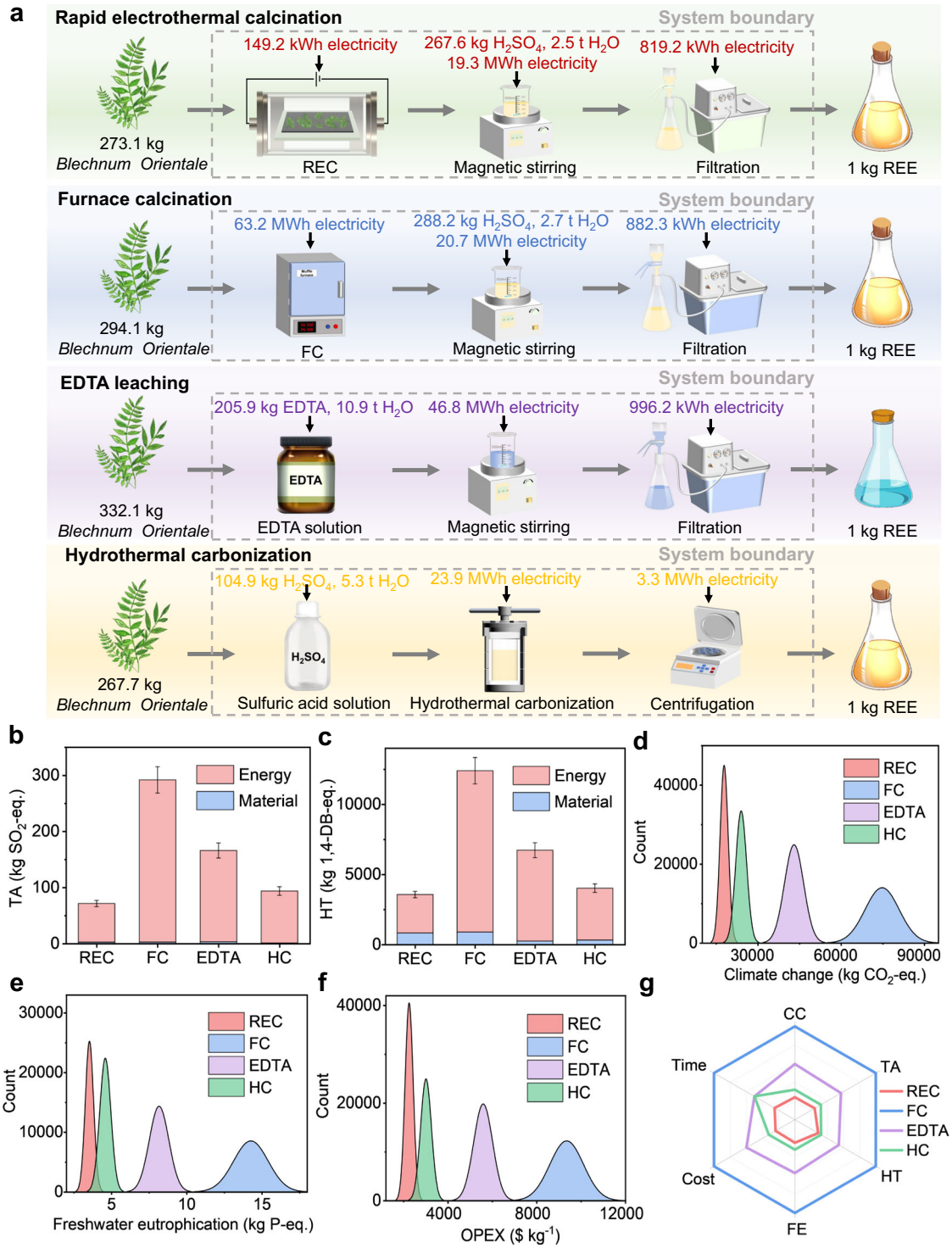

Fig. 5 | Environmental and economic considerations for REE extraction processes. a Process design comparison of REC, FC, EDTA, and HC scenarios for LCA and TEA analysis. **b** Terrestrial acidification comparison. **c** Human toxicity comparison. **d** Climate change comparison utilizing Monte Carlo uncertainty analysis with $N = 50{,}000$ iterations. **e** Freshwater eutrophication comparison utilizing Monte Carlo uncertainty analysis with $N = 50{,}000$ iterations. **f** Operating expenditure (OPEX) comparison utilizing Monte Carlo uncertainty analysis with $N = 50{,}000$ iterations. **g** Comprehensive performance comparison. The scale bars in (**b**, **c**) denote the standard deviation based on Monte Carlo analyses.

consumption, and equipment expenditure, while labor expenses and waste management costs were excluded due to the high dependence on regional economics or plant scale, as well as the challenges in their quantification. Furthermore, the labor expenses across the four processes exhibit minimal divergence. The operating expenditure (OPEX) associated with REC is lower, representing only ~24% of that associated with FC (Fig. 5f, Supplementary Fig. 44, and Supplementary Table 15). The REC approach demonstrates advantages over conventional processes across multiple environmental and economic metrics, as evidenced by radar plot analysis (Fig. 5g).

Scalability of the REC process

The scalability of the REC process is crucial for practical applications. Theoretical analysis indicates that Joule heating is intrinsically scalable, as both current and duration can be adjusted to accommodate larger sample masses while maintaining stable resistance when the heater geometry is proportionally scaled (see Supplementary Note for details). Finite-element simulations confirmed that uniform temperature profiles were maintained as the heater size increased from 1 × 2 cm to 10 × 20 cm and 20 × 40 cm, achieving stable temperatures around 1000 °C under comparable power densities (Supplementary Figs. 64–66).

Laboratory validation further demonstrated consistent performance at the 10 × 20 cm scale, with carbon paper heaters exhibiting stable operation, uniform heating, and no observable hotspots or structural degradation (Supplementary Fig. 63). The morphology after repeated operation confirmed the mechanical stability of the carbon paper at decimeter-scale dimensions. To enhance durability for repeated and long-term use, the heater material was upgraded to a graphite-boat reactor, which maintained structural integrity and electrical performance after dozens of cycles (Supplementary Fig. 58), owing to graphite's superior thermal stability and resistance to shock and corrosion.

Building upon these findings, a pilot-scale REC system has been designed and constructed, operating at comparable power density and exhibiting uniform heating as verified by infrared thermography. Preliminary energy analysis indicates that processing 1 kg of biomass via REC requires 74.0 kWh of electricity, only 25.7% of that needed for the FC process (288.3 kWh), demonstrating the superior energy efficiency and scalability of REC. These results collectively confirm that the REC process can be reliably and efficiently scaled from the gram level to pilot-scale operation, providing a robust foundation for industrial implementation.

Systematic implications for global REE supply

To situate our experimental findings within the context of real-world supply, we examine the potential role of phytomining in the global REE supply chain. Conventional routes such as bastnäsite and ion-adsorption clay can deliver a large-scale supply but are accompanied by high energy consumption, chemical dependence, and environmental externalities. The capital expenditure (CAPEX) of phytomining processes (REC and FC) was quantitatively compared with that of conventional mining routes (bastnäsite and ion-adsorption clay), as illustrated in Supplementary Figs. 45, 46, with detailed descriptions provided in Supplementary Note 3 and Supplementary Tables 16–19. The CAPEX analysis shows that at a processing capacity of 1 t d^{-1}, the recovery costs are estimated at $330.8 for REC, $314.6 for FC, $347.9 for bastnäsite, and $384.4 for ion-adsorption clay. When scaled up to 100 t d^{-1}, these costs decrease to $76.9, $70.4, $126.3, and $95.3, respectively (Supplementary Fig. 47). Monte Carlo simulations further confirm the cost competitiveness of phytomining at an engineering scale (Supplementary Fig. 48–50). In addition, between the two phytomining processes, the combined OPEX and CAPEX of REC were 339.0 k$ t^{-1}, compared with 346.4 k$ t^{-1} for FC, highlighting the comparative benefits of REC in terms of both environmental performance and cost.

Beyond the laboratory scale, the feasibility of phytomining must be situated within the broader context of the global rare earth element (REE) supply chain. As shown in Supplementary Fig. 53, global REE reserves are highly unevenly distributed, with a limited number of dominant mining districts, thereby amplifying geopolitical and trade-related vulnerabilities. This concentration is further reflected in Supplementary Fig. 54, where domestic production in 2024 reveals a strong dependence on a handful of countries, raising concerns for supply security and international equity. At present, the uneven distribution of REE resources poses concerns, as it may heighten international competition and geopolitical tensions, thereby constraining progress towards global climate targets[46]. Ensuring the stability of REE supply chains through effective strategies is therefore critical for supporting a climate-resilient transition[2]. The real-world deployment of phytomining is constrained by biomass supply patterns, land-use and harvesting logistics, and region-specific climatic and policy frameworks[47]. We therefore position REC as a regional, low-carbon, and complementary pathway that can operate in areas with abundant hyperaccumulator resources and a desire to reduce mining externalities, rather than as a direct substitute for large-scale conventional mining. Beyond techno-economic considerations, the deployment of renewable energy–enabled phytomining must be embedded within broader land-use and governance frameworks[48]. At scale, logistical considerations become critical. Land availability, species selection, and harvesting efficiency will determine the practicality of large-scale deployment. The global distribution of fern species richness (Supplementary Fig. 55) illustrates the potential biogeographic resources for phytomining, while also underscoring the importance of aligning site selection with ecological suitability and climate constraints.

Beyond cultivation, the downstream logistics of biomass collection, processing, and chemical management represent important factors that could influence both environmental performance and social acceptance. At scale, the land requirement per unit of REE output becomes a critical factor. Based on our experimental system, approximately 273.1 kg of biomass (0.376 wt% REE) is required to yield 1 kg of REE, implying that even a modest production target of 1000 tonnes of REE annually would require around 2.7×10^5 tonnes of biomass. Assuming typical hyperaccumulator yields of 10–20 tonnes ha^{-1} yr^{-1} (dry weight), this corresponds to 14,000–27,000 hectares of cultivation area, comparable to the land footprint of a medium-sized city. Such figures highlight that scaling phytomining will hinge on land-use efficiency, high-biomass-yielding hyperaccumulators, and optimized cropping systems[49]. Its role is therefore better conceived as a distributed, low-carbon supplement that can contribute to regional supply diversification and environmental remediation[16], rather than as a wholesale replacement of conventional mining. Land availability and access represent primary constraints, as biomass cultivation may compete with food production or ecological conservation goals[50]. Large-scale harvesting also raises challenges related to labor intensity and rural livelihoods[51], highlighting the need for policies that reconcile resource extraction with social sustainability[52]. While REC substantially reduces chemical inputs compared with conventional processes, robust regulatory mechanisms remain necessary to manage residual biomass and prevent unintended ecological impacts[53]. Integrating phytomining into existing agroforestry systems may further mitigate land competition while providing co-benefits for soil restoration and carbon sequestration[54]. Moreover, global equity dimensions must not be overlooked[55]. Considering the broader socio-environmental implications, land-use competition, labor requirements, and equitable access to emerging technologies warrant systematic evaluation. In this context, phytomining must be examined not only as a technical innovation but also as part of a cross-sectoral framework that connects resource security, environmental stewardship, and social fairness. When coupled with global mitigation goals (Supplementary Fig. 56), such integration highlights the potential of phytomining to contribute to both sustainable REE supply and climate-resilient transitions[56]. Addressing such imbalances will require governance structures that integrate land-use agreements, labor standards, and principles of environmental justice[57]. Embedding phyto-metallurgy within broader supply-chain diversification strategies is critical, not only to secure REE supply[13], but also to ensure that technological innovation aligns with sustainability and social responsibility objectives.

Discussion

The integration of REC with phytomining offers a possible approach to address two bottlenecks in conventional biomass processing, energy-intensive thermal degradation[58] and dependence on environmentally hazardous chemical treatments[59]. In the experiments, Fe/Al contamination was effectively restricted to approximately 0.4% through the REC process (Supplementary Fig. 51). This could be attributed to the high reaction temperature (~ 1000 °C), under which Fe and Al were transformed into a leach-resistant silicate or glassy phase (Supplementary Fig. 52). Moreover, the REC treatment achieved a remarkable REE liberation efficiency of up to ~97% in hyperaccumulator ferns. The process also reduces energy demand through direct Joule heating and short treatment times. Preliminary life

cycle assessment (LCA) suggests a 76.1% reduction in carbon emissions compared to conventional furnace calcination, whereas techno-economic analysis (TEA) demonstrates that phytomining not only entails lower CAPEX than industrial bastnäsite and ion-adsorption clay processes, but also achieves lower overall costs relative to conventional FC. These findings highlight REC as a promising strategy for enhancing the sustainability of REE recovery from biomass, though further studies are needed to evaluate its performance across different feedstocks, reactor scales, and operational settings.

By integrating rapid electrothermal calcination with plant-based REE enrichment, this study provides an example of how materials science and environmental engineering approaches can be combined for resource recovery. The use of renewable electricity with low-grade biomass (0.1–0.3 wt% REE) highlights a possible route toward more distributed recovery pathways, though further work is needed to evaluate implications for supply resilience. Future studies should focus on optimizing REC applications across diverse hyperaccumulators and assessing the feasibility of using agricultural residues as potential feedstocks. To enhance economic viability and scalability, future efforts will integrate modular REC reactors with renewable energy sources to slash electricity costs[60], while coupling bioleaching consortia (e.g., *Bacillus cereus*[61], *Bacillus licheniformis*[62], *Novosphingobium*, and *Solirubrobacter*[63]) will reduce acid consumption, cutting reagent expenses and maintaining >90% REE recovery for industrial deployment. At the same time, scale-up development will require careful consideration of heat and mass transfer to ensure homogeneity in larger reactors (Supplementary Note 4). For instance, the graphite boat reactor explored here illustrates one possible design to enhance operational stability (Supplementary Figs. 57, 58). Overall, while phytomining may offer environmental advantages compared to conventional ore processing, additional investigation is essential to assess its technical, economic, and ecological viability before large-scale implementation.

Materials and methods

Materials

The chemicals used were HCl [36 to 38 wt%, ≥99%, Macklin], HNO_3 (65 to 68 wt %, ≥99%, Macklin), H_2SO_4 [98 wt %, ≥99%, Sinopharm Chemical Reagent Co., Ltd.], $HClO_4$ (70 to 72 wt%, ≥99%, Sinopharm Chemical Reagent Co., Ltd.), HF (48 wt %, ≥99%, Sinopharm Chemical Reagent Co., Ltd.), $MgCl_2$ (99%, Acmec), CH_3COONa (99%, Amethyst), $Na_4P_2O_7$ (99%, Macklin), NH_2OH (50 wt %, Acmec). The *Blechnum orientale* samples and *Dicranopteris linearis* samples were collected from Guangdong province, China, and provided to our laboratory [see Acknowledgments]. The *Blechnum orientale* samples and *Dicranopteris linearis* samples were ground into powders using a grinder (Dade, DF-15). The carbon paper was purchased from Fuel Cell Store (Toray Carbon Paper 060). Carbon paper is chosen as the heater because it has appropriate resistance for heating, and it is a highly graphitized material that is stable up to 3000 °C.

REC system and process

In preparation for REC treatment, *Blechnum orientale* and *Dicranopteris linearis* biomass samples were mechanically pulverized using a commercial grinder (Dade, DF-15). For controlled thermal processing, precisely measured 500 mg aliquots of plant material were uniformly distributed on carbon paper substrates. The substrate assembly was integrated with a capacitive discharge system, where controlled pulse current inputs induced rapid resistive heating of the carbon paper. The reaction was conducted in a pulsed electric heating reactor, comprising four core components: power supply, control panel, reaction chamber, and data acquisition system (Supplementary Fig. 59). A stage heating mode was employed for temperature control. Initial power parameters were set at a power supply voltage of 36 V and power supply current of 83 A, followed by configuration of target temperatures and reaction durations (Supplementary Fig. 60). With a carbon heater resistance of ~1 Ω, different temperature and time gradients are applied. The Raw BO was directly heated instantly by contact heat conduction. Using BO as feedstock, experiments were performed at 500, 600, 700, 800, 900, and 1000 °C, with reaction times of 1 s, 10 s, 20 s, and 60 s (totaling 24 experimental sets). Optimized conditions yielded maximum extraction efficiency at 1000 °C for 20 s. During this reaction, real-time power supply voltage and current were shown in Supplementary Fig. 61, and the corresponding reaction power profile was displayed in Supplementary Fig. 62. As demonstrated in Fig. 1f, real-time thermal monitoring revealed synchronous temperature profiles between the carbon paper heater and sample matrix during the millisecond-scale heating phase. We have achieved the upscaled experiments with a carbon heater size of 10 cm× 20 cm (Supplementary Fig. 63), and numerical simulations confirmed further scaling feasibility to even larger sizes (Supplementary Figs. 64–66). The REC process (Fig. 1g) initiated rapid oxidative combustion of organic constituents in the ambient atmosphere, achieving peak combustion temperatures sufficient for complete volatile organic compound (VOC) decomposition. This combustion process selectively preserved REE through differential thermal stability mechanisms: (1) organic cellular matrices binding REE underwent complete pyrolysis, while (2) target REE with elevated boiling points remained thermally stabilized on the carbon substrate. Post-treatment analysis confirmed efficient extraction of REE-enriched residues through simple mechanical detachment from the carbon paper interface.

Sample digestion, leaching, ICP-OES measurement, and various forms of REE content measurement

For the *Blechnum orientale* samples and *Dicranopteris linearis* samples, acid-extractable REE content measurement and total REE quantification were conducted. For total quantification, ~250 mg samples were digested in 10 ml concentrated HNO_3 (15 M) at 120°C for 1 h of digestion under microwave. The sample was filtered using a sand core funnel (class F) and diluted using ultrapure water for ICP-OES measurement. For H_2SO_4 leaching, ~1 g samples (Raw BO, Raw DL, Activated BO, Activated DL, Calcinated BO, and Calcinated DL) were digested in ~10 ml H_2SO_4 (0.1 M) at 90 °C for 1 h. After digestion, the sample was filtered using a sand core funnel (class F) and diluted to ~100 ml using ultrapure water for ICP-OES measurement. The pH-dependent leaching dynamics were investigated by using 1, 0.1, 0.01, and 0.001 M H_2SO_4 at pH 0.3, 0.7, 1.8, and 2.5, respectively, as the leaching agents.

The ICP-OES measurement was conducted using a ThermoFisher iCAP 6300 system. The detection limits for REE are in the range of 0.5 to 5 parts per trillion (ppt). The REE mixture standard was used (Macklin; 16 elements; 10 mg L^{-1} each; Sc, Y, La, Ce, Pr, Nd, Sm, Eu, Gd, Tb, Dy, Ho, Er, Tm, Yb, and Lu in 5 wt% % nitric acid). In our analyses, the standards were in the concentration range of 1 to 1000 parts per billion. All the analyzed samples were carefully diluted into the concentration range, which is at least two orders of magnitude higher than the detection limit of quantification. All the samples were measured three times to determine the SDs.

A sequential extraction routine was used to evaluate the REE fractions in Raw BO, Activated BO, and Calcinated BO[40,41]. The ion-exchangeable fraction (step I) was extracted using $MgCl_2$ solution (pH = 7 ± 0.2), the carbonate binding fraction (step II) was extracted using CH_3COONa solution (pH = 5 ± 0.2), the humic acid binding fraction (step III) was extracted using $Na_4P_2O_7$ solution (pH = 10 ± 0.2), the Fe-(hydr)oxide fraction (step IV) was extracted using NH_2OH–HCl solution (pH = 2 ± 0.2), the strong organic binding fraction (step V) was extracted using H_2O_2 + HNO_3, and finally the residual fraction (step VI) was extracted using HNO_3–HF–$HClO_4$ solution.

Characterization

The SEM images were obtained by using a Czech TESCAN MIRA LMS SEM system at 5 kV. XRD was collected using a Bruker D8 Discover system. Crystalline size was calculated using the Scherrer equation, while crystallinity was determined by dividing the integrated area of the crystalline diffraction peaks by the total integrated area of the XRD pattern. XPS spectra

were taken using a Thermofisher Nexsa XPS system under the base pressure of 5×10^{-9} Torr. Elemental XPS spectra were collected using a step size of 0.1 eV with a pass energy of 26 eV. All of the XPS spectra were calibrated by using the standard C 1 s peak at 284.8 eV. TGA was conducted in N_2 at a heating rate of 10 °C min^{-1} up to 800 °C by using a Q5000IR Simultaneous TGA/DSC from TA instruments. Calcination was conducted using the Mafu furnace in the air (SA2-6-12TP).

Life-cycle assessment

The environmental impacts were evaluated via life cycle assessment (Supplementary Note 2). Four scenarios were considered in this study: FC, EDTA, HC, and our REC (Fig. 5a). The LCI entries were converted into environmental impacts using the ReCiPe 2016 methodology[23]. The ecoinvent v3.8 database was employed as the background system, prioritizing China-specific datasets wherever available; when regional data were absent, global averages were used as substitutes. The energy efficiency of REC was quantitatively compared with conventional FC, EDTA, and HC under optimized operational parameters. The REC system achieved rapid thermal activation through resistive Joule heating. It demonstrated a heating rate of 100 °C s^{-1}, reaching the target temperature of 1000 °C within 10 s. In contrast, the furnace calcination process required prolonged thermal exposure: heating from ambient to 550 °C at 10 °C min^{-1} (equivalent to 0.167 °C s^{-1}) over 55 min, followed by a 3-hour isothermal retention at 550 °C. In addition, due to differences in extraction efficiency, there are also differences in the amount of BO and material consumption. A detailed analysis of the four processes is provided in Supplementary Note 2. Monte Carlo simulations were implemented for sensitivity analyses. It is important to note that the LCA conducted in this study is preliminary; in actual production, the water requirement for separation and current efficiency may vary due to optimization efforts. These factors could introduce uncertainty into the LCA analysis.

Techno-economic analysis

The economic feasibility of the REC process was evaluated via technoeconomic analysis (Supplementary Note 3). The required chemical reagents were sourced based on domestic market prices in China, with specific prices for relevant items detailed in Supplementary Table 14. The evaluation in this work does not account for the price of spent materials or the labor cost. The overall process cost was calculated by projecting energy consumption and potential benefits under the proposed operating conditions. Economic performance indicators such as net present value (NPV), internal rate of return (IRR), and payback period (PBP) were not included in this preliminary analysis but could be incorporated into future studies for a more comprehensive evaluation. It is also acknowledged that scaling the laboratory-based process to an industrial level may introduce additional technical and economic challenges, which could affect the overall feasibility and profitability of the proposed process.

Data availability

The data supporting the findings of this study are available within the article and its Supplementary Information. Other relevant data are available from the corresponding author, B.D. (dengbing@tsinghua.edu.cn), upon reasonable request.

Received: 21 December 2025; Accepted: 23 January 2026;
Published online: 02 February 2026

References

1. Jowitt, S. M., Mudd, G. M. & Thompson, J. F. H. Future availability of non-renewable metal resources and the influence of environmental, social, and governance conflicts on metal production. *Commun. Earth Environ.* **1**, 1–8 (2020).
2. Wang, P. et al. Regional rare-earth element supply and demand balanced with circular economy strategies. *Nat. Geosci.* **17**, 94–102 (2024).
3. Borst, A. M. et al. Adsorption of rare earth elements in regolith-hosted clay deposits. *Nat. Commun.* **11**, 1–15 (2020).
4. Lee, J. C. K. & Wen, Z. Pathways for greening the supply of rare earth elements in China. *Nat. Sustain.* **1**, 598–605 (2018).
5. Vahidi, E., Navarro, J. & Zhao, F. An initial life cycle assessment of rare earth oxides production from ion-adsorption clays. *Resour. Conserv. Recycl.* **113**, 1–11 (2016).
6. Meng, X. et al. Effective recovery of rare earth from (bio)leaching solution through precipitation of rare earth-citrate complex. *Water Res* **233**, 119752 (2023).
7. Xin, C. et al. Strengthening rare earth and inhibiting aluminum leaching in magnesium salt-acetic acid compound system from ion-adsorption type rare earth ore. *Sep. Purif. Technol.* **334**, 126070 (2024).
8. Wang, G. et al. A green and efficient technology to recover rare earth elements from weathering crusts. *Nat. Sustain.* **6**, 81–92 (2023).
9. Strzelecki, A. C. et al. Fluocerite as a precursor to rare earth element fractionation in ore-forming systems. *Nat. Geosci.* **15**, 327–333 (2022).
10. Prommer, H. Towards sustainable rare-earth-element mining. *Nat. Sustain.* **6**, 13–14 (2023).
11. Chour, Z. et al. Basis for a new process for producing REE oxides from Dicranopteris linearis. *J. Environ. Chem. Eng.* **8**, 103961 (2020).
12. Zheng, H. X. et al. Plasma-membrane-localized transporter NREET1 is responsible for rare earth element uptake in hyperaccumulator dicranopteris linearis. *Environ. Sci. Technol.* **57**, 6922–6933 (2023).
13. Rabbani, M., Taqi Rabbani, M., Muthoni, F., Sun, Y. & Vahidi, E. Advancing phytomining: Harnessing plant potential for sustainable rare earth element extraction. *Bioresour. Technol.* **401**, 130751 (2024).
14. Jally, B. et al. A new method for recovering rare earth elements from the hyperaccumulating fern Dicranopteris linearis from China. *Miner. Eng.* **166**, 106879 (2021).
15. Dinh, T., Dobo, Z. & Kovacs, H. Phytomining of rare earth elements – A review. *Chemosphere* **297**, 134259 (2022).
16. Dang, P. & Li, C. A mini-review of phytomining. *Int. J. Environ. Sci. Technol.* **19**, 12825–12838 (2022).
17. Anderson, C.W. N., Brooks, R.R, Stewart, R.B. & Simcock, R. Harvesting a crop of gold in plants. *Nature* **395**, 553 (1998).
18. Wang, L. et al. Field trials of phytomining and phytoremediation: A critical review of influencing factors and effects of additives. *Crit. Rev. Environ. Sci. Technol.* **50**, 2724–2774 (2020).
19. Qin, B. et al. Vacuum pyrolysis method for reclamation of rare earth elements from hyperaccumulator Dicranopteris dichotoma grown in contaminated soil. *J. Clean. Prod.* **229**, 480–488 (2019).
20. Jalali, J., Gaudin, P., Ammar, E. & Lebeau, T. Bioaugmentation coupled with phytoextraction for the treatment of Cd and Sr, and reuse opportunities for phosphogypsum rare earth elements. *J. Hazard. Mater.* **399**, 122821 (2020).
21. Deng, B. et al. Rare earth elements from waste. *Sci. Adv.* **8**, 1–9 (2022).
22. Luong, D. X. et al. Gram-scale bottom-up flash graphene synthesis. *Nature* **577**, 647–651 (2020).
23. Zhu, X. et al. Continuous and low-carbon production of biomass flash graphene. *Nat. Commun.* **15**, 3128 (2024).
24. Choi, C. H.W. et al. Flash-within-flash synthesis of gram-scale solid-state materials. *Nat. Chem.* **16**, 1831–1837 (2024).
25. Deng, B., Eddy, L., Wyss, K. M., Tiwary, C. S. & Tour, J. M. Flash Joule heating for synthesis, upcycling and remediation. *Nat. Rev. Clean. Technol.* **1**, 32–54 (2025).
26. Cheng, Y. et al. Electrothermal mineralization of per- and polyfluoroalkyl substances for soil remediation. *Nat. Commun.* **15**, 6117 (2024).
27. Hong, C., Tang, Q., Liu, S., Kim, H. & Liu, D. A two-step bioleaching process enhanced the recovery of rare earth elements from phosphogypsum. *Hydrometallurgy* **221**, 106140 (2023).

28. Grosjean, N. et al. Accumulation and fractionation of rare earth elements are conserved traits in the Phytolacca genus. *Sci. Rep.* **9**, 18458 (2019).
29. Wang, H. et al. Uptake and transport mechanisms of rare earth hyperaccumulators: A review. *J. Environ. Manag.* **351**, 119998 (2024).
30. Cui, X. et al. A review on the thermal treatment of heavy metal hyperaccumulator: Fates of heavy metals and generation of products. *J. Hazard. Mater.* **405**, 123832 (2021).
31. Doroshenko, A. et al. Using: In vivo nickel to direct the pyrolysis of hyperaccumulator plant biomass. *Green. Chem.* **21**, 1236–1240 (2019).
32. Khanna, R., Ellamparuthy, G., Cayumil, R., Mishra, S. K. & Mukherjee, P. S. Concentration of rare earth elements during high temperature pyrolysis of waste printed circuit boards. *Waste Manag* **78**, 602–610 (2018).
33. Park, S. & Liang, Y. Bioleaching of trace elements and rare earth elements from coal fly ash. *Int. J. Coal Sci. Technol.* **6**, 74–83 (2019).
34. Chen, Y., Fabbricino, M., Benedetti, M. F. & Korshin, G. V. Spectroscopic in situ examination of interactions of rare earth ions with humic substances. *Water Res* **68**, 273–281 (2015).
35. Önal, M. A. R. et al. Recycling of NdFeB magnets using nitration, calcination and water leaching for REE recovery. *Hydrometallurgy* **167**, 115–123 (2017).
36. Wang, Y. et al. Experimental investigation on pyrolysis of coking waste salts: Mechanism of organic compounds removal and salt agglomeration. *J. Environ. Manag.* **388**, 125974 (2025).
37. Jowitt, S. M., Werner, T. T., Weng, Z. & Mudd, G. M. Recycling of the rare earth elements. *Curr. Opin. Green. Sustain. Chem.* **13**, 1–7 (2018).
38. Talik, E. et al. XPS characterisation of neodymium gallate wafers. *J. Alloy. Compd.* **377**, 259–267 (2004).
39. Bai, B. et al. The influence of pretreatment on the bond-breaking rules during pyrolysis of Shengli lignite and the construction of macromolecular structure model. *J. Anal. Appl. Pyrolysis* **191**, 107215 (2025).
40. Huang, J. et al. Groundwater controls REE mineralisation in the regolith of South China. *Chem. Geol.* **577**, 120295 (2021).
41. Denys, A. et al. Evaluation of selectivity of sequential extraction procedure applied to REE speciation in laterite. *Chem. Geol.* **559**, 119954 (2021).
42. Liu, W. S. et al. Phytoextraction of rare earth elements from ion-adsorption mine tailings by Phytolacca americana: Effects of organic material and biochar amendment. *J. Clean. Prod.* **275**, 122959 (2020).
43. Zhao, X. et al. Covalent bonding structures of eight oil shales and the characteristics of bond cleavage during the pyrolysis process. *Fuel* **370**, 131821 (2024).
44. Deng, B. et al. Flash separation of metals by electrothermal chlorination. *Nat. Chem. Eng.* **1**, 1–26 (2024).
45. Qiao, Y., Wen, X., Liu, S., Lv, S. & He, L. Stochastic analysis for comparing life cycle carbon emissions of hot and cold mix asphalt pavement systems. *Resour. Conserv. Recycl.* **212**, 107881 (2025).
46. Franks, D. M., Keenan, J. & Hailu, D. Mineral security essential to achieving the Sustainable Development Goals. *Nat. Sustain.* **6**, 21–27 (2023).
47. Rabbani, M. et al. Advancing circular economy through phytomining: Critical mineral recovery from mine tailings and environmental impact assessment. *ACS Sustain. Chem. Eng.* **13**, 11335–11347 (2025).
48. Owen, J. R. et al. Energy transition minerals and their intersection with land-connected peoples. *Nat. Sustain.* **6**, 203–211 (2023).
49. Erkmen, A. N., Ulber, R., Jüstel, T. & Altendorfner, M. Towards sustainable recycling of critical metals from e-waste: Bioleaching and phytomining. *Resour. Conserv. Recycl.* **215**, 108057 (2025).
50. Naidu, R., Biswas, B., Nuruzzaman, M. & Singh, B. K. Bioremediation of heavy metal(loid)s in agricultural soils and crops. *Nat. Rev. Bioeng.* https://doi.org/10.1038/s44222-025-00345-y (2025).
51. Aska, B. et al. Mining, biodiversity and social conflict in the renewable energy transition. *Nat. Rev. Biodivers.* **1**, 597–614 (2025).
52. Giljum, S. et al. Metal mining is a global driver of environmental change. *Nat. Rev. Earth Environ.* **6**, 441–455 (2025).
53. Johnson, R. Biotransformations for bioremediation. *Nat. Chem. Biol.* **19**, 1287–1289 (2023).
54. Díaz, A. M. et al. Phytoremediation strategies for the reclamation of tailings and mining soils in an active open-pit site. *Environ. Res.* **275**, 121464 (2025).
55. Wei, Y. M. et al. Navigating energy transition solutions for climate targets with minerals constraint. *Nat. Clim. Chang.* **15**, 833–841 (2025).
56. Nature Editorial Team. Net-zero carbon pledges must be meaningful. *Nature* **592**, 8 (2021).
57. Rahimpour, S. et al. Selected social impact indicators influenced by materials for green energy technologies. *Nat. Commun.* **15**, 1–13 (2024).
58. Hu, Y., Zhang, B., Guo, Q., Wang, S. & Lu, S. Characterization into environmentally persistent free radicals formed in incineration fly ash and pyrolysis biochar of sewage sludge and biomass. *J. Clean. Prod.* **373**, 133666 (2022).
59. Moramarco, A., Ricca, E., Acciardo, E., Laurenti, E. & Bracco, P. Cellulose extraction from soybean hulls and hemp waste by alkaline and acidic treatments: An in-depth investigation on the effects of the chemical treatments on biomass. *Polym. (Basel)* **17**, 1220 (2025).
60. Peramaiah, K. et al. Unassisted photoelectrochemical CO2 reduction by employing III–V photoelectrode with 15% solar-to-fuel efficiency. *Carbon Energy* **669**, 1–10 (2025).
61. Li, X. et al. Indigenous microbial influence on REE enrichment and fractionation in South China weathering crusts: Insights from experimental simulations. *Chem. Geol.* **663**, 122263 (2024).
62. Cheng, Y. et al. Resource recovery: Adsorption and biomineralization of cerium by Bacillus licheniformis. *J. Hazard. Mater.* **426**, 127844 (2022).
63. Cebekhulu, S. et al. Role of indigenous microbial communities in the mobilization of potentially toxic elements and rare-earth elements from alkaline mine waste. *J. Hazard. Mater.* **466**, 133504 (2024).

Acknowledgements

We express our gratitude to the Guangzhou Institute of Geochemistry, Chinese Academy of Sciences, for providing the *Blechnum orientale*. The funding of the research was provided by the National Natural Science Foundation of China (No. 92475112, B.D.; No. 51978375, J.L.), National Key Laboratory Special Fund Project of China Minmetals Corporation (Grant No. 2025GZGJ02, B.D.), the Beijing Natural Science Foundation (No. F251042, B.D.), and the Central Leading Local Science and Technology Development Fund (YDZJSX2024D002, B.D.).

Author contributions

B.D. and M.X. conceived the idea. M.X. conducted most of the experiments and characterization. T.W., E.F., and Z.H. assisted with the experiments. M.X. conducted the LCA and TEA with the help of T.W. Z.Y. conducted the numerical simulation. Q.M., W.L., and R.Q. provided hyperaccumulators and offered useful suggestions to the experimental design. M.X., B.D., and J.L. wrote the manuscript. This work was supervised by B.D. and J.L. All aspects of this work were overseen by B.D. All authors revised and commented on the final version of this article.

Competing interests

The authors declare no competing interests.

Additional information

Supplementary information The online version contains supplementary material available at https://doi.org/10.1038/s43246-026-01089-x.

Correspondence and requests for materials should be addressed to Bing Deng or Jianguo Liu.

Peer review information This manuscript has been previously reviewed at another Nature Portfolio journal. The manuscript was considered suitable for publication without further review at Communications Materials.